Numerical simulation of the Helicon Double Layer Thruster Concept

Marco Manente*
CISAS University of Padua, Padova Italy
Johan Carlsson†
Tech-X corporation, Boulder CO USA
Ivano Musso‡
CISAS University of Padua, Padova Italy - ISTI-CNR Pisa Italy
Cristina Bramanti§
Advanced Concept Team ESA ESTEC Noordwijk - The Netherlands
Daniele Pavarin,¶ and Francesco Angrilli‖
CISAS University of Padua, Padova Italy

During last years some laboratories obtained current free helicon double layers in experiments with both electropositive and electronegative gases. The current free double layer has potential application as a plasma thruster. Although considerable progress has been made, at the present time a number of aspects related to this phenomenon are still only partially understood. This paper presents results obtained by numerical simulation of double layer formation, stability and characteristics and explores the applicability of this concept to a space mission. The analysis has been conducted using a combination of 1-D and 2-D numerical codes.

After the modelization of helicon source, the code is applied to simulate a simple plasma thruster.

Nomenclature

A	the cross surface of the cell revolution
A_{Exh}	geometrical exhaust area
cp	coefficient
c_s	coefficient
E_{TH_i}	threshold energy for i-th reaction
e	electron charge
I_{sp}	specific impulse
K_i	reaction rate for i-th specie
k_B	Boltzmann constant
L_{Exh}	ions lost at the exhaust
m	particle mass
m_{ion}	ion mass
n	plasma density

*Post-Doc Fellow, Department of Mechanical Engineering, University of Padua, Via Venezia 15 35131 Padova Italy
†Research Scientist, Tech-X corporation, 5621 Arapahoe Ave Suite A, Boulder, CO 80303
‡PhD student, Department of Mechanical Engineering, University of Padua, Via Venezia 15 35131 Padova Italy - ISTI-CNR Pisa Italy
§ESA technical officer, Advanced Concept Team ESTEC - DG-PI, Keplerlaan 1 - 2201 AZ Noordwijk - The Netherlands
¶Researcher, Department of Mechanical Engineering, University of Padua, Via Venezia 15 35131 Padova Italy
‖Full professor, Department of Mechanical Engineering, University of Padua, Via Venezia 15 35131 Padova Italy

n_e electron density
n_i density of i-th specie
n_j density of the specie involved in the i-th reaction
P_{Abs} deposited power into plasma
P_{Exh} power loss associated with the electron and ion flux at the exhaust
P_i power lost in the i-th reaction
P_W power lost at the exhaust
r radius of magnetic lines tube
r_i radius of the detachment cell
T particle temperature
T_e electron temperature
u_B ion Bohm's velocity
V_a average axial velocity inside the detachment cell
V_e plasma volume
z position
Γ_{Exh_i} flux loss term due to the particle flow through the exhaust for the i-th specie
Γ_i^l flux loss term due to plasma process for the i-th specie
Γ_i^s flux source term due to plasma process for the i-th specie
Γ_{W_i} flux loss term due to particle recombination at wall for the i-th specie
σ cross section

I. Introduction

Double-layers (DLs) are electrostatic structures able to support a potential jump in a narrow spatial region of plasmas. DLs have been studied intensively interpreting and reproducing magnetospheric, solar plasma phenomena.[1,2] The motions of charged particles determine the internal structure of a DL and, by the net charge distribution, its electric field. In the most general DL structure both free and reflected electrons and ions are required. The electric field acts as a barrier for the reflected particles while the accelerated ones emerge after it as energetic beams. The current is carried by the free particles. Usually DLs studied by laboratory tests and theoretical models require an electron current or an external imposed electric field. Sometimes their formation is ascribed to the evolution of plasma instabilities. Perkins[3] demonstrated the possibility for current-free DL. These DLs required the presence of trapped ions to exist. Chan,[4] few years later, made experiments in his triple-plasma device were ion-acoustic DLs, similar to the Perkins solution, were found. Recently Charles and Boswell have reported about a current-free DL obtained by a helicon-source plasma expansion along a diverging magnetic field. Their findings can lead eventually to development of innovative space propulsion system.[5–7] Similarities were met by independent researchers: Hairapetian,[8] Cohen,[9] Sun[10,11] and Plihon;[12,13] while a first 1D-MCC-PIC model was tested by Meige and Boswell.[14] Chen[15] recently proposed that Double Layers observed in plasmas expanding along the magnetic fields in laboratory simulations of plasma thrusters for space propulsion, are actually single layer and are predictable from classical sheath theory normally applied to boundaries with only one assumption: electrons are Maxwellian. Comparing the Boswell, Sun and Plihon experiments and, with some differences, the Hairapetian one, we can address that the DL formation is mainly due to the plasma expansion and subsequent density reduction and that it happens when a particular "dimensional" threshold, defined by chamber pressure, source density, source-chamber dimension and expansion rate, is reached. Taking into account the Hairapetian and Chan approaches one could suggest that, in particular cases, the helicon produces an electron flux able to start the DL formation process, as they have reported or imposed in their experiments.

From a preliminary analysis of current ongoing experiments the following points may represent the key factors on DL formation and stability:

Charge separation: Analyzing the DL experiments it appears that charge separation could be one of the main mechanism on DL formation. Perkins wrote that the hypothesis of ion trapping is necessary for his solution of current-free DL, while Hairapetian explained that his experiment as due to a high energy electrons. Finally from the stable DL case, Plihon measured an electronegative discontinuity near the DL (high electronegative plasma after the potential jump), probably a sort of charge trapping.

Effect of the distribution function: The DL formation could be linked to high energetic electrons on the tail of the distribution. Hairapetian reported evidence of high energy electrons during the DL formation: the source electrons were considered non Maxwellian (Maxwellian + high energy tail). Boswell deduced the DL formation during plasma break-down, when high energy electrons are present. However, recently Charles and Chen proposed that Maxwellian distribution should be sufficient to explain DL formation.

Effect of plasma expansion: Effect of plasma expansion: Both Chen and Meige propose to link Double Layer formation to the mechanism of ion density reduction due to vacuum-expansion along the magnetic lines.

The modeling approach here after proposed is based on three different numerical models: a) a global numerical model of the plasma source, b) a 1-D PIC code of the entire system , c) a 2-D PIC code of the entire system. The global model is used to simulate the plasma source behavior, it provides the source ionization rate, plasma density and electron temperature to the other two codes. A 1-D code named PPDL was developed specifically for this purpose. It is a hybrid code with Boltzmann electrons and drift-kinetic ions, inclusion of dominant 2-D effects and high computational efficiency through implicit nonlinear Boltzmann solver. The 2-D code used was XOOPIC, freely available from University of California at Berkeley. With XOOPIC it was necessary to perform fully electromagnetic simulations with kinetic electrons, resulting in long computational times. A combined approach therefore proved very useful where the 1-D code was used to rapidly screen many different experimental conditions and to identify the right boundary condition. The 2-D code was then used to refine the 1-D results. This paper will present the 1-D PIC (PPDL) code which has been expressly developed and inspired by Chen[15]and Meige[14] works: Maxwellian electrons combined with plasma density reduction due to expansion into vacuum and floating boundary conditions. The 1-D analysis has been accompanied by some 2-D simulations, made with an existing software, to compare the 1-D results and verify the exhaust flux properties and divergence.

II. Global model of plasma source

The plasma balance equations, for particles and energy, have been written for describing uniformly distributed plasma inside of a region determined by the magnetic field configuration. The neutral interaction with plasma has been considered in this work by coupling a 0-dimensional gas-dynamic model of the entire system with a global plasma model of the source. The plasma balance equations, for particles and energy, have been written for describing uniformly distributed plasma inside of a region determined by the magnetic field configuration. The interactions that are taken into account in the model are:

- Neutral density reduction due to ionization;
- neutral dissociation (molecular specie-atom species);
- zero dimensional gas dynamic analysis behaviour in the plasma source and in the vacuum chamber;
- wall recombination and volume recombination in the main vacuum chamber.

The particle balance equations for the ionized particles and electrons are written in a particle flux form, (particles/seconds m^3). The general form for the balance equations of charged particles is:

$$\frac{dn_i}{dt} = \Gamma_i^s - \Gamma_i^l - \Gamma_{W_i} - \Gamma_{Exh_i} \tag{1}$$

Γ_i^s is for the i-specie the source term due to plasma processes, Γ_i^l is the loss term due to plasma processes, Γ_{W_i} is for the i-specie the loss term due to particle recombination at the wall (the particle diffuses through the wall sheath before reaching the wall), Γ_{Exh_i} is the loss term due to the particle flow through the exhaust. The reaction rates were obtained averaging the cross section for the specific reaction over a maxwellian distribution:[16]

$$K_i = \left(\frac{m}{2\pi kT}\right)^{3/2} \int_0^\infty \sigma(v) v \exp\left(-\frac{mv^2}{2kT}\right) 4\pi v^2 dv \tag{2}$$

where T is the particle temperature in eV, m is the partile mass and σ the cross section. Wall losses are calculated as in.[17–19] Ions lost at the exhaust are calculated as :

$$L_{Exh} = n_i \cdot u_B \cdot A_{Exh} \cdot cp \tag{3}$$

$$u_B = \sqrt{\frac{kT_e}{m_i}} \tag{4}$$

u_B term is the ion Bohm's velocity and A_{Exh} is the geometrical exhaust area and cp takes into account the ratio among the real exhaust velocity (derived numerically through 1-D code or experimentally) and the ion Bohm velocity.

To calculate the electron temperature, the power balance equation has been written as follows (units: W/m^3)

$$\frac{P_{Abs}}{Ve} = \frac{d}{dt}\left(\frac{3}{2} \cdot e \cdot n_e \cdot T_e\right) + \sum P_i + P_W + P_{Exh} \tag{5}$$

P_{Abs} is the deposited power into the plasma that is assumed to be known. e is the electron charge, T_e is the electron temperature, V_e again the plasma volume. P_i terms are the power lost in the i-reaction. The general formula is:

$$P_i = K_i \cdot E_{TH_i} \cdot n_e \cdot n_j \tag{6}$$

where K_i is the rate constant for the specific reaction, E_{TH_i} the threshold energy for the i-reaction,[20] n_e the electron density, n_j the density of the specie involved in the i-reaction. P_W is the power lost at the wall due to the electron-ions flow. P_{Exh} is the power loss associated with the electron and the ion flux at the exhaust, assuming that the escaping velocity is the ion-Bohm velocity multiplied by c_s. Experimental results[21] indicate the presence of a hot tail in the electron population in hydrogen and helium discharge. This distribution has been modelled summing two maxwellian distributions: one with the temperature of the bulk of the plasma and one with the temperature of the hot tail. The results of a evolutionary algorithms optimization applied to the source simulation is used in PIC code to model the source and the expansion of plasma generated.

III. Development of PPDL code

The PPDL is a modified version of an existing 1-D PIC named PadPIC, a Particle in Cell[22] plasma simulator. The main features of PPDL are:

- Drift-kinetic ions, where the magnetic moment is assumed to be an adiabatic invariant. The drift kinetic equation of motion
- The expansion of the magnetic field is considered
- Boltzmann electrons, assuming Maxwellian distribution and inertialess.
- Floating boundary conditions.
- Plasma generation is simulated through a source term.

The advantage of Boltzmann electrons is that electron time scale (plasma and gyro periods) do not have to be resolved, but on the other side it requires a non-linear Poison solver to determine the electrostatic potential. With the hybrid Boltzmann electron/drift-kinetic ion approach, the time step is only limited by ion period which is two orders of magnitude larger than electron plasma period and ion gyro period, which can become very short in a strong magnetic field, is removed. Thus, PPDL is very fast and efficient and still capable of simulating the relevant physics. To better fit the experimental set-up the presence of magnetic field is simulated by the analytic solution of a field generated by one or more solenoids. The gradient of the magnetic field is also calculated analytically and used for adding the ∇B velocity to the drift-kinetic ions. The dilution of the charge density due to the expanding magnetic field has also been incorporated into the non linear Poisson solver

We consider a plasma of radius r_0, density n_0, and temperature T_e created in a uniform field B_0 and then injected into a region of expanding field lines. For plasma frozen to the field lines.

The expansion of $B(z)$ and $n(z)$ plasmas along the magnetic field is also simulated using the relation

$$\frac{n}{n_0} = \frac{B}{B_0} = \left(\frac{r_0}{r}\right)^2 \tag{7}$$

where r(z) is the radius of magnetic lines at position z.

III.A. PPDL results

The monodimensional code PPDL was performed with several conditions and geoemtries for thrusters to identify the critical parameters. It use the source modeled in the previous step and studies the expansion of the system. The results are summarized in the follow (all values are in S.I except temperature in eV): the model is similar to Charles experiment, with different boundary condition: the right boundary can be floating so the system is sometime mirrored to permit to obtain the floating wall near the source or far from the source. In some simulation we observed an ion beam velocity around 1.4 times the ion Bohm velocity

Temperatures

Ion and electron temperatures

Obviously the maximum potential is increased by the temperature due to sheath effect: as shown in the Figure 1.

The ratio between ΔV and V_{max} increase with V_{max}, so it seems that some advantage can derive increasing the temperature. A larger difference between electron and ion temperature increases the potential drop as in Figure 2, where we use $T_e = T_i$ =60 eV (`MAlongtime3`)and T_e=60 eV T_i=1 eV (`MAlongtime7`).

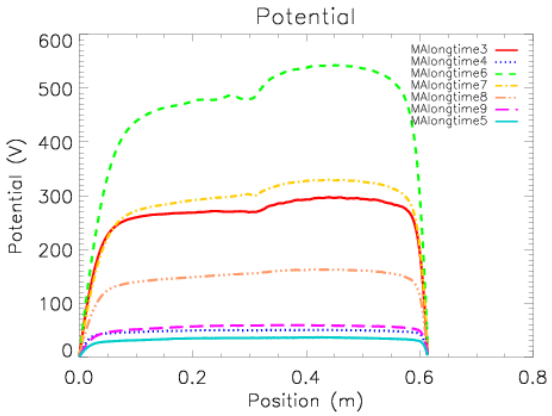

Figure 1. Potential as function of the position at different ion and electron temperatures: `MAlongtime3`: T_e=T_i=**60 eV** `MAlongtime4`: T_e=**10** T_i=**10 eV** `MAlongtime6`: T_e=**100** T_i=**1 eV** `MAlongtime7`: T_e=**60** T_i=**1 eV** `MAlongtime8`: T_e=**30** T_i=**1 eV** `MAlongtime9`: T_e=**10** T_i=**1 eV** `MAlongtime5`: T_e=**6** T_i=**.1 eV**

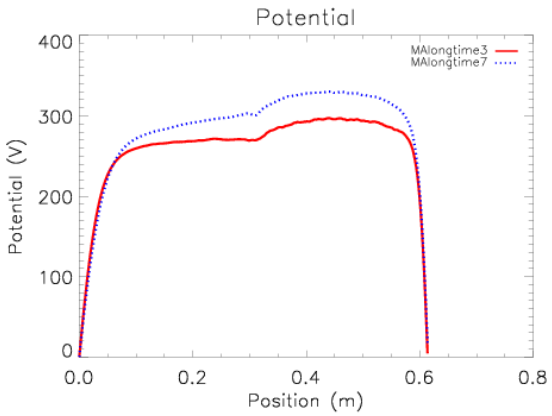

Figure 2. Potential as function of the position at different ion and electron temperatures: `MAlongtime3`: T_e=T_i=**60 eV** and `MAlongtime7`: T_e=**60eV** T_i=**1 eV.**

Magnetic field

Coil configuration

We used two different configurations of magnetic field: the first one uses line without inversion, with a long solenoid also in the expansion camera as shown in Figure 3.

The second one uses two solenoid only over the source as shown in figure 4.

We use a plasma frozen to the magnetic lines, in order to use only the magnetic lines that do not turn. PPDL uses the first of the magnetic tube that does not invert: in that case we can define the radius of the larger close magnetic tube for each z and we can calculate the density dilution with eq. 7

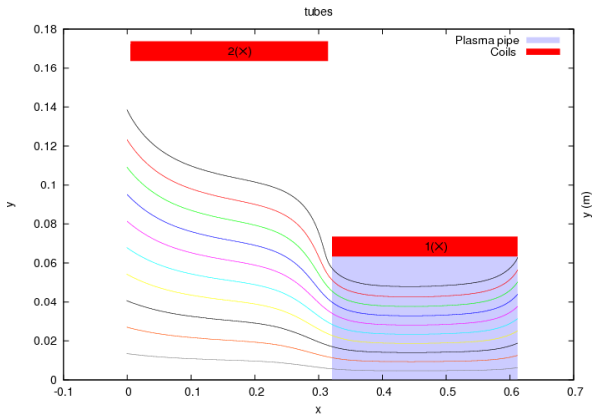

Figure 3. Magnetic field lines with solenoid in expansion chamber

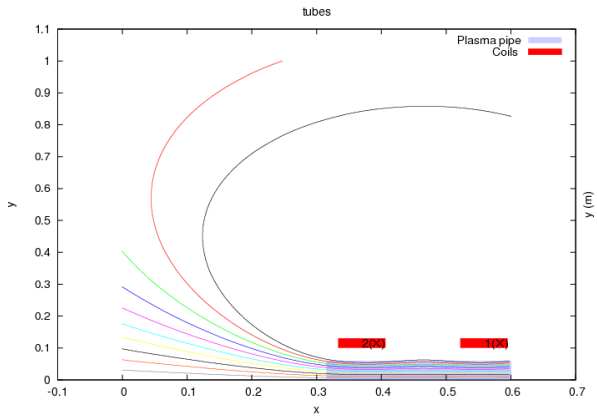

Figure 4. Magnetic field lines with two solenoid only over the source

Magnetic field strength

There's no significant difference if we simply increase the wire current to achieve a different magnetic field strenght, from B_{max}=150G to B_{max}=300G

Plasma source

Source position

The position of source rate is very important for the localization of potential drop as shown in figure 5 where the `CIxcomp_invpd14` has the source in the original position (0.35-0.55 m), `CIxcomp_invpd15` has the source between 0.45 to 0.55 m and `Cixcomp_invpd16` between 0.35 to 0.45 m.

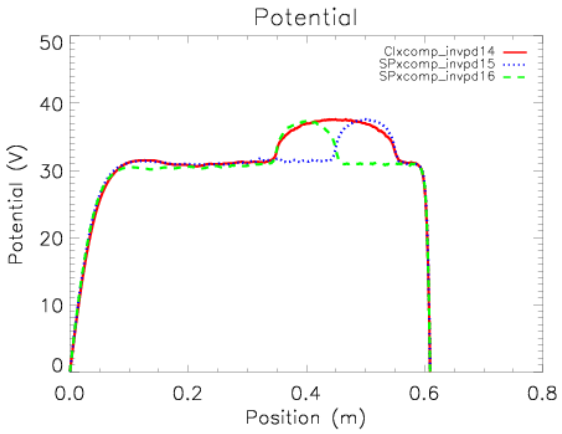

Figure 5. Potential profile for different length and position of the plasma source

Neutral pressure

The collision probability between plasma and neutrals, calculated with the method explained above, shows no collisions for pressure around 0.1-3 mTorr (so there is no influence of neutral by collisions). Probably the neutral pressure influences only the source rate of plasma production.

Density

From the comparison of the same simulations with different plasma density we can see that the influence of density is not important for the potential drop as in figure 6 and 7. All the curves of the figure 6 are

different simulation but with same density. The same potential profile is plotted in Figure 7 with a different simulations density.

The density can change the kinetic energy for the detachment

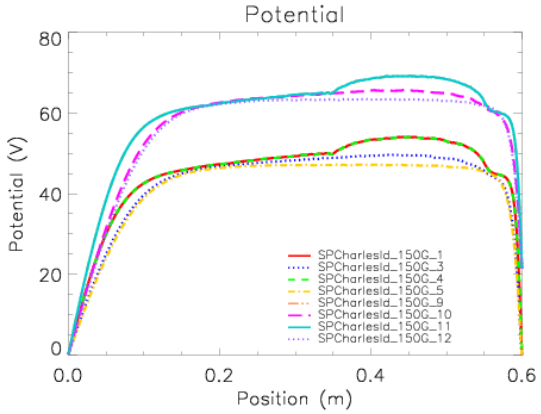

Figure 6. Potential profile of several simulation: all simulations present density = 10^{14}

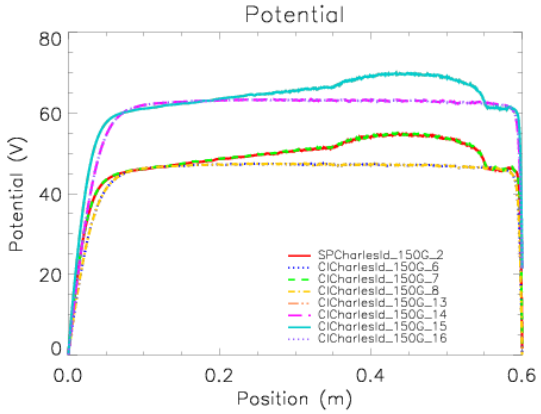

Figure 7. Potential profile of several simulation: all simulations present density = 10^{15}

DC bias

The influence of DC bias is only related to the value of maximum potential as shown in Figure 8 but the potential drop is practically unaffected In Figure 9 the lower curves (`SPESA_Bosdld4` SR=5e18 and `CIESA_Bosdld13` SR = Mant.) are at DC bias 0V-0V. The upper curves (`SPESA_Bosdld5` SR=5e18 and `CIESA_Bosdld14` SR = Mant.) are at DC bias 10V-0V

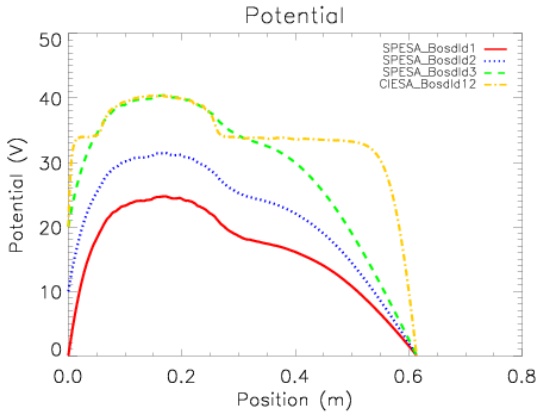

Figure 8. Dc Bias influence:`SPESA_Bosdld1` (Dc bias 0V) `SPESA_Bosdld1` (Dcbias 10V) `SPESA_Bosdld1` (Dc bias 20V) `CIESA_Bosdld12` (Dc bias 20V and SR = Mant.)

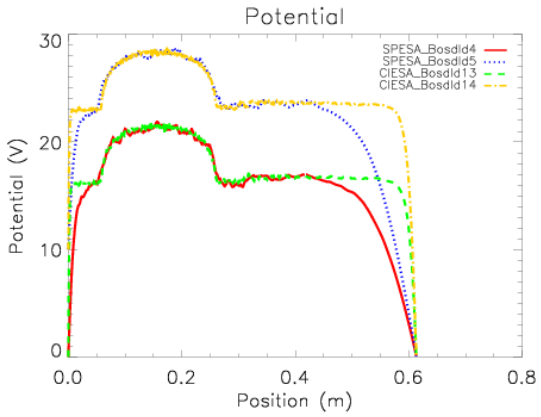

Figure 9. DC bias influence: The lower curves (`SPESA_Bosdld4` SR=5e18 and `CIESA_Bosdld13` SR =Mant.) are at 0V-0V DC bias. The upper curves (`SPESA_Bosdld5` SR=5e18 and `CIESA_Bosdld14` SR = Mant.) are at 10V-0V Dcbias

Gas

We simulate both Hydrogen and Argonas propellant. Argon shows a maximum potential higher than hydrogen, as shown in figure 10, but ΔV is similar. The specific impulse reached by argon is around 650s and hydrogen reached 3800 s

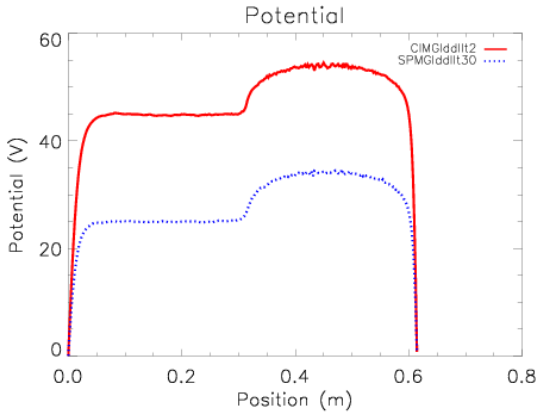

Figure 10. comparison between Argon (`CIMGlddllt2`) and Hydrogen (`SPMGlddllt30`)

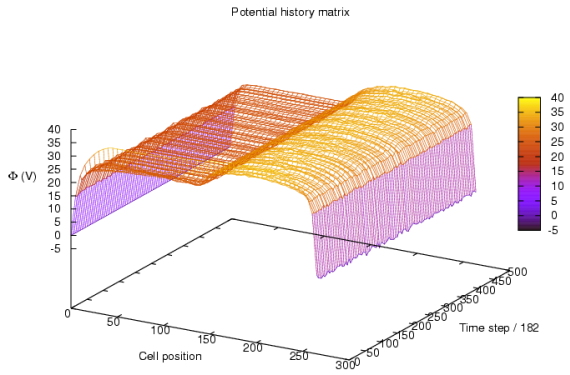

Figure 11. Time history of potential profile

Time stability

The time stability of potential drop is shown in Figure 11 for a time length of 1 ms. The graph shows the potential profile time history, and it is possible to see that the profile remains constant for all the time after a short transient period.

System Length

No effect of the system length has been observed as shows in figure 12

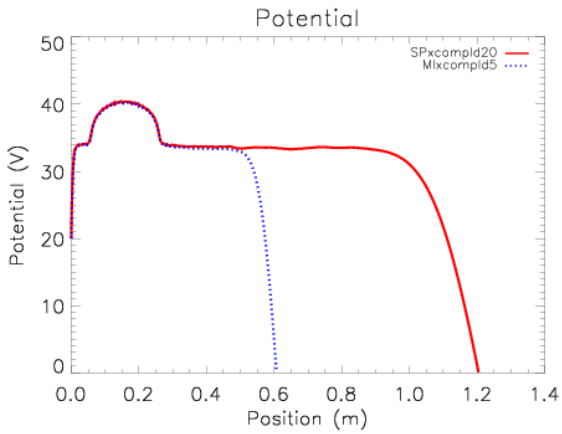

Figure 12. Same simulation with different system length

IV. OOPIC CODE

The 2-D simulations used a stable existing software which has been applied to several configurations. We drawn the geometry and shape of the model following the set up utilized by Charles and Boswell. Since floating walls were not possible because none of the OOPIC objects fulfil this characteristic, we reproduced the helicon source with the nearer objects allowed by the software: surfaces with dielectrics, conductors at constant potential or open (not confining) properties. The results has been compared with the PPDL simulations.

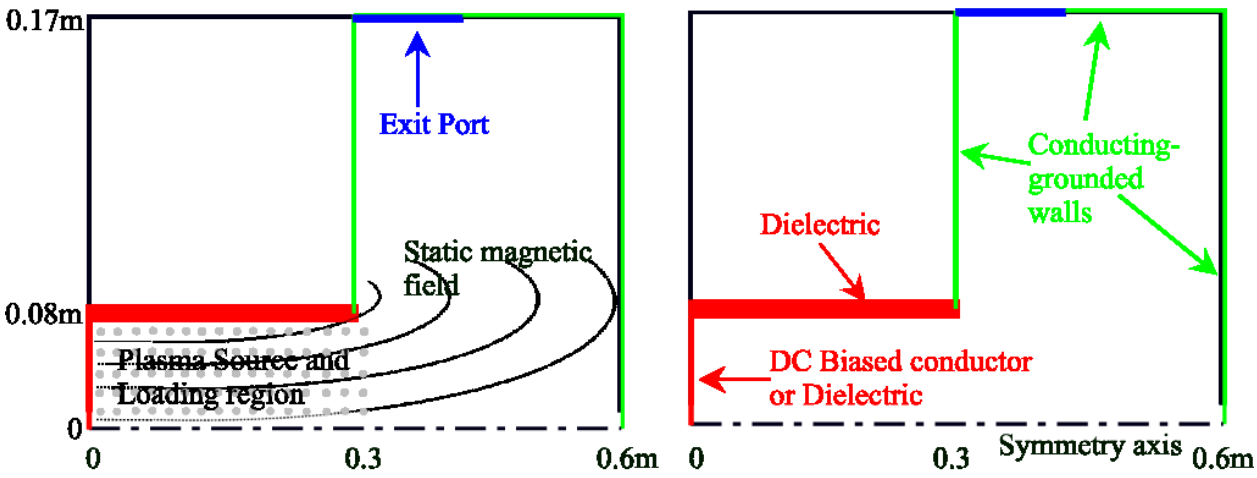

Figure 13. Geometry configuration used on OOPIC simulations

IV.A. 2-D model description

In this section the results obtained by the simulations performed by OOPIC (Object-Oriented Particle-In-Cell) code, open-source Berkeley (University of California), are reported. OOPIC is a 2D-3V relativistic electromagnetic PIC code. The object-oriented paradigm provides an opportunity for advanced PIC modelling, increased flexibility, extensibility and efficiency.[23] OOPIC includes 2-dimensional orthogonal grid: cartesian (x,y) or cylindrically symmetric (r,z) and moving window, as well as electrostatic and electromagnetic solves and relativistic particles. The boundaries can be determined at runtime and include many models of emitters and collectors. Because the dependence on the azimuthal angle is not expected to be relevant for DL experiments, we can use a 2-D r-z cylindrical PIC simulation. The code can handle an arbitrary number of species, particles, and boundaries. It also includes Monte Carlo collision (MCC) algorithms for modelling collisions of charged particles with a variety of neutral background gasses. The figure 13 presents the geometry configuration used for the simulations.

The plasma conditions have been characterised by the definition of ions and electrons densities exiting from the source tube. This is a versatile approach because we could change the parameters, simulating plasma expansion in different conditions. The resolution of the particles motion is done under electrostatic assumption. Few particles are immediately loaded into the source region, to represent the high energy electrons produced during the breakdown and to start without a empty region, while the most are created during the simulation. The plasma production is represented by the OOPIC PlasmaSource object. The particles are created at a given rate in a rectangular area and with Maxwellian velocity distribution and a changeable density distribution. The plasma production density is defined in order to model the typical helicon source behaviour: maximum density near r=0 and after the tube half (see Fig 14).

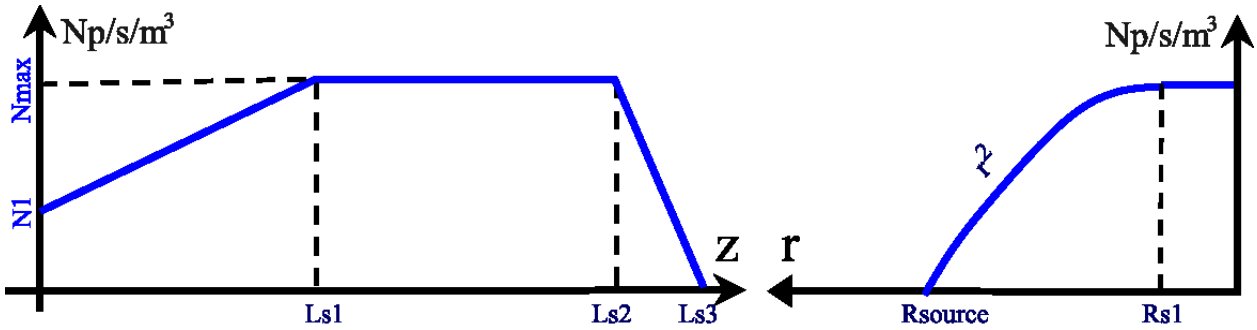

Figure 14. Plasma rate density distribution: Ls3=Lsource=30cm, Rs1=1.5cm and N1=Nmax/3

The static magnetic field has been calculated by solving the equations for circular filamentary coils in 2-D. The two solenoids have been located around the source tube at r=12-13cm, axial positions of 1 and

20cm and length of 8cm. The result is a function with two peaks of 150G, as reported by Charles, and it has been saved in a text file which could be imported by OOPIC at the initialization of the simulation.

IV.B. OOPIC results

The simulations we have made have been divided in four parts:

1. Low density ($\sim 10^{12} m^{-3}$), with open (non confining) source walls
2. Medium density ($\sim 10^{13} m^{-3}$)
3. High density ($\sim 10^{14} m^{-3}$), with halved cell dimension (1024x256 cells of 0.6x0.6 mm)
4. Medium density, with long diffusion chamber to simulate out space (1024x256 cells of 1.2x1.2mm) and evaluate detachment

For each case we have performed several simulations changing the main border conditions (magnetic field, neutral density, electron and ion temperatures and wall electric properties).

In particular we have tested the case of DC biased left wall. At low density we have analyzed the cases with 0, 10 and 20V dc biased left wall while at high density we have increased the bias to obtain plasma potentials inside the source as near as possible to the measured values, that were near 70V. The simulated ions are hydrogen, in order to have light particles that can fill the diffusion chamber in a time sufficiently short to be reproduce with full PIC simulations. For biased and non-confining source walls, the potential jump appeared around 10-15V, so similar to the one seen during the experiments. The potential drop reported by Charles was 2-4 cm long, during our simulations the width was at least three times bigger. For low density plasmas the potential decreases from 10-15V to almost 5V in not less than 10cm and this happens only when the left source wall could increase its potential by applying a biased or not confining surface (Figure 15). The high density simulations show an axial potential more smooth, where the values can decrease of 10V in 20cm. In any case the results confirm the presence of high energetic ions inside the diffusion chamber at radius lower than the helicon tube width. This family of particles have a velocity near two times the ions sound speed, as reported by Charles.

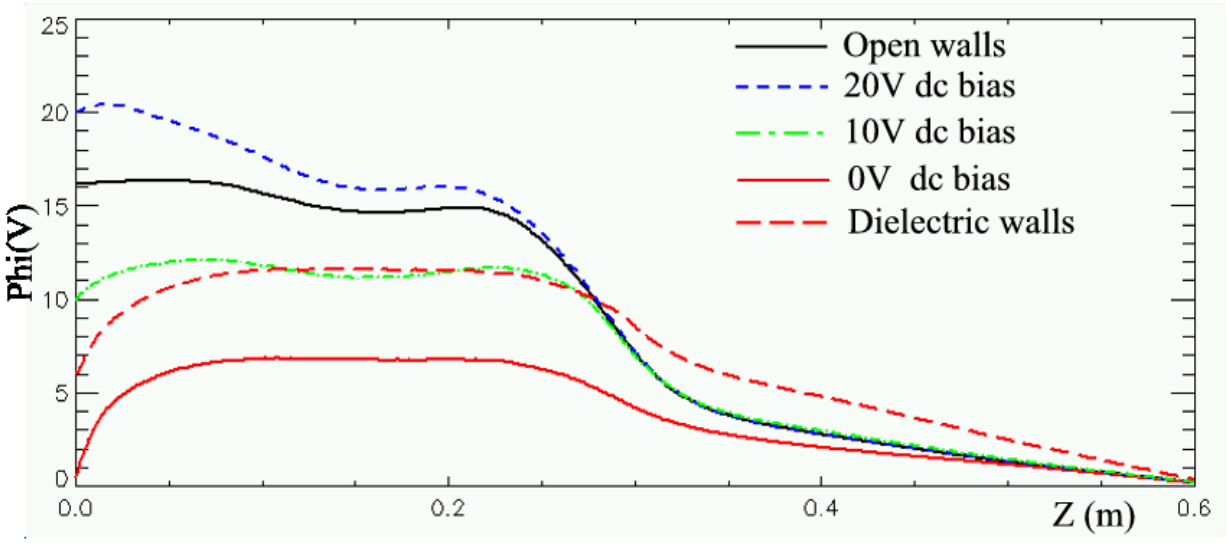

Figure 15. Axial plasma potential for the low density simulations after 15μ s

V. Comparison between the experiments and models results

The codes have been used for reproducing the 1-D PIC results of Meige et AL. and the ANU experiments.[14,24–26] The distribution functions are Maxwellian and density has been decreased to enlarge the

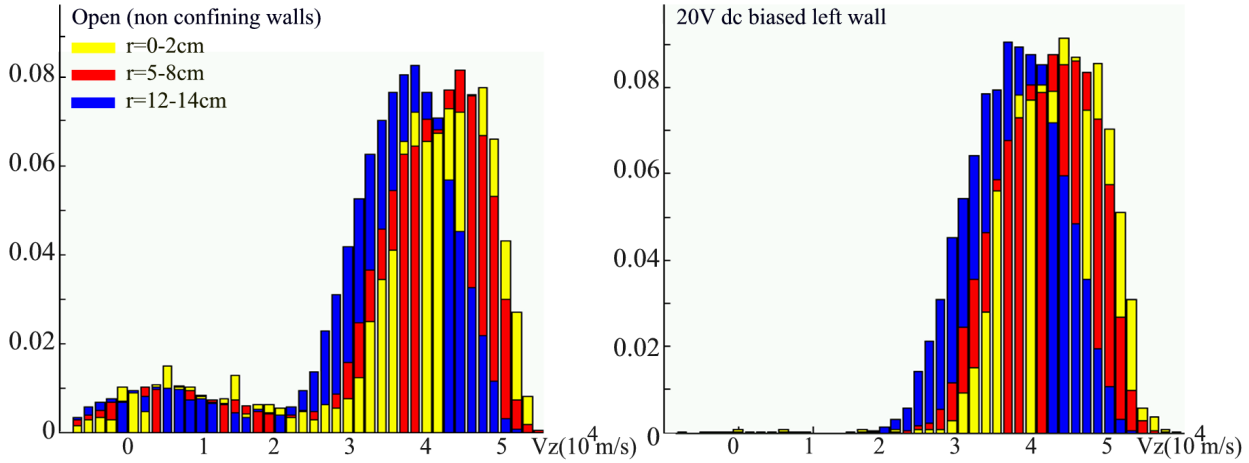

Figure 16. Ions relative density as function of the axial velocity and radius and for z=40-45cm (10cm outside the helicon tube). The height of each bar represents the relative density of ions having that velocity.

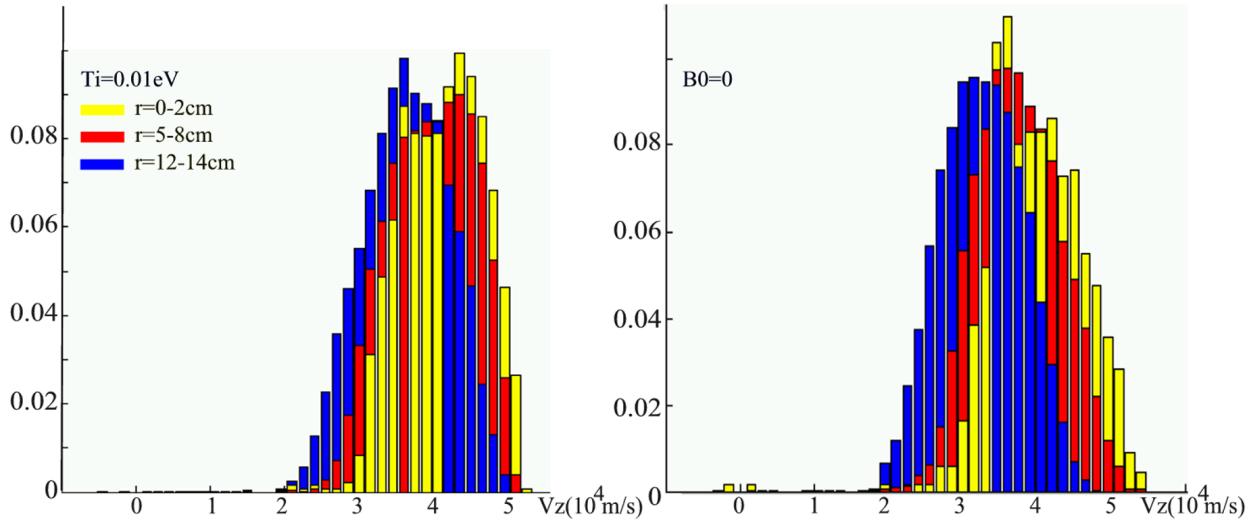

Figure 17. Ions relative density as function of the axial velocity and radius and for z=40-45cm (10cm outside the helicon tube). The height of each bar represents the relative density of ions having that velocity.

Debye sphere and allowing fewer cells to be used in the simulation. PPDL results have been compared with the OOPIC simulations and the measurements made by Charles. The axial potential calculated by OOPIC is lower than the one computed by PPDL for similar border conditions (Fig 18), but we found significant agreements between the two models. Both show potential jumps between source and diffusion chamber around 10V, not far from the 15-20V obtained at ANU. The length of this potential variation is around 10cm for PPDL and 50%-80% bigger for OOPIC, in any case larger than the measured one which is less than 5cm long. Great similarities between simulations and measurements have been met for the velocity distribution functions 10-20cm outside the source tube. The two peak function shown by Charles and modulated by changing some border conditions, in particular electron temperature, electric potential of the left wall and neutral pressure, has been reproduced by the models. See Figure 16 and Figure 17.

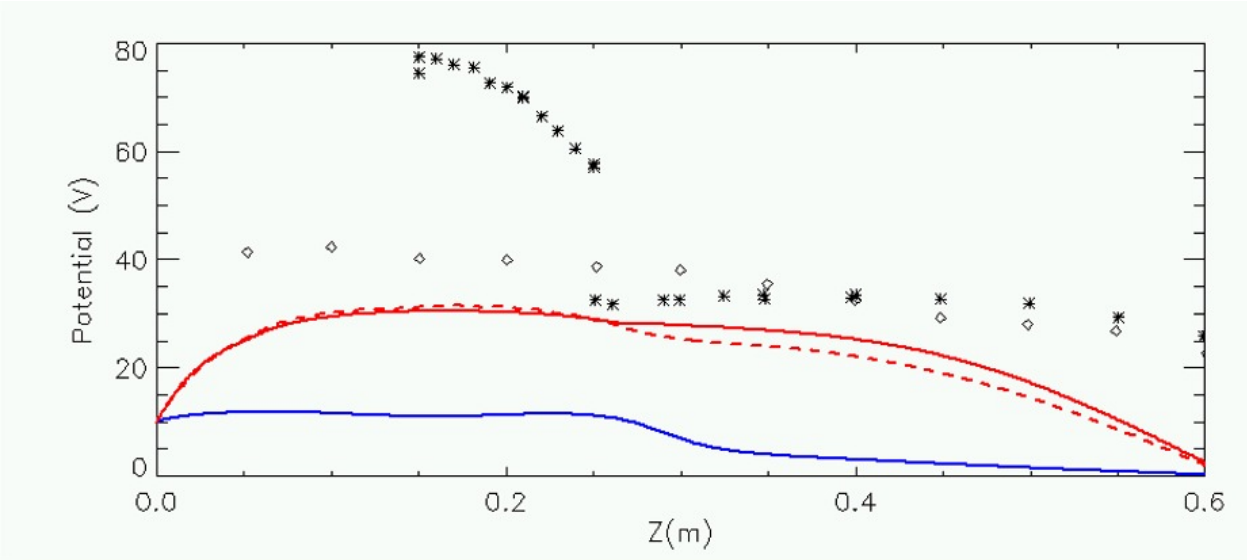

Figure 18. Simulations with source rate of $5 \cdot 10^{17} m^{-3} s^{-1}$ and duration of $15 \mu s$. The lower continued line is the OOPIC simulation, PPDL simulations are the upper continued line (red), the (red) dashed line is the simulation of $150 \mu s$. The left source wall is a 10V dc biased. Stars are the Charles measurements with DL (high magnetic field and low neutral pressure) and squares are the measurements without DL.

VI. Thrust performance evaluation

The thrust has been calculated with OOPIC for four different detachment lines. Those lines have been selected considering the axial positions from which the direction of the ions' velocity starts to be constant. We supposed that the distance from the helicon tube exit where the detachment takes place grows with the axial position. It is considered greater than 20cm at the tube axis and almost constant but more than 60cm for $r > 30$cm. The thrust has been calculated through the formula:

$$T = \sum mNV_a^2 A \tag{8}$$

iterated for every r_i along the supposed detachment line,where $m - ion$ is the ion mass, N is the density of ions inside the detachment cell at radius r_i, V_a is the average axial velocity inside the detachment cell and A is the cross surface of the cell revolution: $A = \pi[(r_i + dr)^2 - r_i^2]$. Therefore for all the cells that follow the selected line we have evaluated the ions' density, which is a default output of OOPIC, and the average ions' axial velocity. The result is a thrust around $4 \cdot 10^{-7}$ N; it has been obtained comparing three simulations made with T_e=8eV, 70V dc biased left wall and diffusion chambers 1m long with different electrical properties. The simulations we made reached a density, inside the source tube, around $5 \cdot 10^{13} m^{-3}$, the source rate has been set between 10^{18} and $3 \cdot 10^{18} m^{-3} s^{-1}$ and the gas is hydrogen.

The specific impulse (Is) can be calculated by means of the formula:

$$I_{sp} = (\sum NV_a)/(\sum Ng) \tag{9}$$

again iterated along the supposed detachment line and where g is the gravitational acceleration. The calculation show a specific impulse between 2500 and 3500s, which is consistent with an average axial exhaust

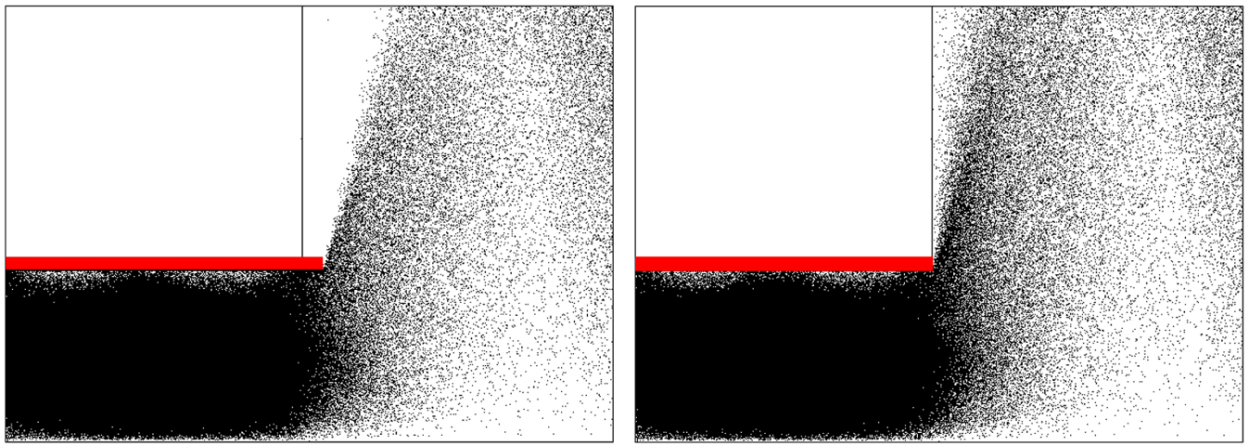

Figure 19. Ions trajectories for 20V dc bias left wall (right) and the same case but with a 2cm longer dielectric tube (left)

velocity of approximately $4 \cdot 10^4 m/s$ (1.5-2 times the ions sound speed) and a partial divergence of the flux (Fig 19).

VII. High power scaling up

Although in an early stage of laboratory experimentation, results indicate that there exists a potential for helicon-type radio-frequency plasma thrusters to operate at high power levels to produce a high continuous thrust, moderate to high specific impulse and reasonable efficiency (up to 60%).[27] This performance makes them an attractive prospect for propelling large spacecraft requiring high delta-V and reasonable mission durations. This type of thruster has, in fact, the additional advantage of requiring no high-current cathode, acceleration grids or neutraliser that presently limit the operating lifetime in other electric thrusters, thus they would appear suitable for very high total impulse missions. Mission applications include human/cargo Mars missions to Mars, robotic missions with large science payloads to orbit the outer planets and their moons or even to deflect near-Earth asteroids from Earth-impacting trajectories.

VIII. Conclusions

The models gives a good description of the physics of the thruster: this makes it possible to simulate the plasma behaviour in the desired configuration and to determine the efficiency and thrust performance. Comparison with experimental results shows that 1-D PIC code underestimate ion beam acceleration by 30% the 2-D PIC code by 10% . The integrated numerical models set-up (global model, 1-D PIC code , 2-D PIC code) allow for helicon-thruster design and detailed analysis.

Acknowledgments

The authors wish to thank Dr. Cinzia Giacomuzzo and Dr. Simone Rocca for their support. This research has been supported by ESA-ARIADNA program

References

[1]M. A. Raadu, "Particle Acceleration Mechanisms in Space Plasmas", Phys. Chem. Earth (C), Vol. 26, No. 1-3, pp.55-59, 2001

[2]M. Raadu, "The physics of double layers and their role in astrophysics", Physics Reports 178, No2, 1989, pp25-97.

[3]F.W. Perkins and Y.C. Sun "Double Layers without current" Phys. Rev. Lett. 46, 115 (1981)

[4]C. Chan, M.H. Cho, N. Hershkowitz, T. Intrator, " Experimental observation of slow ion acoustic Double Layers" Phys. Rev. Lett. 57, 3050 (1986)

[5]C. Charles, R.W. Boswell, "Laboratory evidence of a supersonic ion beam generated by a current-free "helicon" double-layer". Phys. Plasmas 11, 1706-1714 (2004).

[6]C. Charles, "Hydrogen ion beam generated by a current-free double- layer in a helicon plasma". Applied Physics Letters 84, 332-334 (2004)

[7]C. Charles and R.W. Boswell, "Current-free double-layer formation in a high -density helicon discharge". Applied Physics Letters 82, 1356 -1358 (2003).

[8]G. Hairapetian, R. Stenzel, "Particle dynamics and current-free double layer in an expanding, collisionless, two - electron-population plasma", Physics of Fluids B: Plasma Physics, 3, 4, p899, (1991)

[9]S. Choen, N. Siefert, S. Stange, "Ion acceleration in plasmas emerging from a helicon-heated magnetic mirror device", Physics of Plasma, v10, N6, p2593, (2003)

[10]X. Sun, C. Biloiu, R. Hardin, "Parallel velocity and temperature of Ar ions in a expanding, helicon source driven plasma", v13, p359, (2004)

[11]X. Sun, A. Keesee, C. Biloiu, C. Charles, R. Boswell, "Observations of ion-beam formation in a current- free double layer", Physical Rev Letters, v95, 025004, (2005)

[12]N. Plihon, C. Corr, P. Chabert, "Double layer formation in the expanding region of an inductively coupled electronegative plasma", Applied Physics Lett, v86, 091501, (2005)

[13]N. Plihon, C. Corr, P. Chabert, "Periodic formation and propagation of double layers in the expanding chamber of an inductive discharge operating in Ar/SF6 mixture", Journal of Applied Phys, v98, 023306, (2005)

[14]A. Meige, R. W. Boswell, C. Charles "One-dimensional Particle-in-Cell simulation of a current- free double-layer in an expanding plasma" Physics of plasmas 12, 052317 (2005)

[15]F.Chen "Physical mechanism of current free double layer", Physics of plasmas 13,2006

[16]M.A. Lieberman "Principle of Plasma Discharges and Material Processing" New York Wiley 1994

[17]C. Suwon, "A self consistent global model of neutral gas depletion in pulsed helicon plasmas", Physics of plasmas, vol 6, Jan 1996, pp. 359-365.

[18]R. Zorat, "Global model of a radio frequency H2 plasma in DENISE", Plasma Sources Sci Tech 9 (2000) 161-168.

[19]C. Lee "Global model of Ar, O2, Cl2, and Ar/O2 high-high density plasma discharges", J.Vac.Sci.Tech. A 13(2) Mar/Apr 1995.

[20]R.K. Janev "Elementary Processing Hydrogen Helium Plasmas"Springer Verlag, 1987

[21]M.I. Panevsky "Characterization of the Resonant Electromagnetic Mode in Helicon Discharges" PhD Thesis, University of Texas at Austin 2003

[22]Birdsall C., Langdon A. "Plasma Physics via computer simulation" Iop, Bristol, 1991

[23]J.P. Verboncoeur, A.B. Langdon and N.T. Gladd, "An Object -Oriented Electromagnetic PIC Code", Comp. Phys. Comm., 87, May11, 1995, pp. 199-211.

[24]Nicolas Plihon, Pascal Chabert, Jean-Luc Raimbault "Helicon Double Layer Thruster Concept for High Power NEP Missions", ESA Contract Number: 18852/05/NL/MV Final report.

[25]Roger Walker Nicolas Plihon, Pascal Chabert, Jean-Luc Raimbault "Experimental Studies of Helicon Double Layers for Future High Power Plasma Propulsion" 42nd AIAA/ASME/SAE/ASEE Joint Propulsion Conference & Exhibit 9 - 12 July 2006, Sacramento, California AIAA 2006-4844

[26]C. Charles, R.W. Boswell, P. Alexander, C. Costa, O. Sutherland, L. Pfitzner, R. Franzen, J. Kingwell, A. Parfitt, P.E. Frigot, J. Gonzalez del Amo, E. Gengembre, G. Saccoccia, R. Walker, "Helicon Double Layer Thrusters" 42nd AIAA/ASME/SAE/ASEE Joint Propulsion Conference & Exhibit 9 - 12 July 2006, Sacramento, California AIAA 2006-4844

[27]T. Ziemba, J. Carscadden, J. Slough, J. Prager, R. Winglee, "High Power Helicon Thruster", 41 st AIAA/ASME/SAE/ASEE Joint Propulsion Conference & Exhibit, AIAA 2005-4119